OPEN ACCESS
JOURNAL OF ADVANCED DIELECTRICS
Vol. 13, No. 3 (2023) 2243003 (7 pages)

DOI: 10.1142/S2010135X22430032

Domain wall state diagram for $SrTiO_3/BaTiO_3$ superlattice structures*

Yimei You, Fengjuan Yang and Pingping Wu†
Department of Materials Science and Engineering
Xiamen Institute of Technology
Xiamen, Fujian 361021, P. R. China
The Higher Educational Key Laboratory for Flexible Manufacturing
Equipment Integration of Fujian Province, Xiamen Institute of Technology
Xiamen, Fujian 361021, P. R. China
†pingpingwu@xit.edu.cn

Received 31 October 2022; Revised 15 December 2022; Accepted 6 February 2023; Published 3 April 2023

The domain wall structure of ferroelectric/paraelectric superlattices can be much more complex due to the influence of the superlattice stacking structure, the in-plane strain induced by the substrate and environmental temperature. In this study, we employed a phase field model to investigate the domain wall state of the $SrTiO_3/BaTiO_3$ superlattice structure. The domain wall thickness for the $SrTiO_3/BaTiO_3$ layer was measured using a hyperbolic function. Based on the simulation results, here, we show a domain wall state diagram to distinguish the hard and soft domain states. The polarization profiles across hard/soft domain walls were illustrated and analyzed. Our simulation results offer a useful concept for the control of the domain wall state in the ferroelectric superlattice.

Keywords: Domain wall; superlattice; stacking structure; polarization distribution; phase field model.

1. Introduction

In recent years, ferroelectric superlattice structure attracted great attention due to its domain structures and its ferroelectric properties can be finely adjusted through the substrate, stacking structure and environmental temperature.[1–9] Moreover, the topological textures discovered in the ferroelectric nanostructures and superlattice, including polar vortices,[10,11] vortex/anti-vortex pairs,[12–14] meron/skyrmion[15,16] and bubble-like structures,[17] demonstrating these findings are of practical importance in view of increasing applications in high-density information devices.

To many ferroelectric application aspects, the domains accompanying the domain walls play an essential role in the switching properties and strongly affect the domain structure evolution.[18–22] In thin film/superlattice structures, the structure of the domain wall can be quite complex[18,21] and the domain wall width can strongly influence the domain wall mobility.[23,24] In Luk'yanchuk *et al*.'s work,[25–28] an ultra-thin 180° domain wall was generated with Kittel approximate solution at low temperatures, and the flat polarization profile introduces "hard domains" in thick ferroelectric films. If the superlattice structure is heated to a temperature close to Curie temperature T_c, a sinusoidal polarization profile was observed and a soft domain state appears.

Despite the obvious importance of temperature, the domain wall structure also can be influenced by the superlattice stacking structure and its grown-on substrate, only a few simulation studies concerning superlattice stacking structure and temperature dependence have been performed. In our previous study,[29,30] for $SrTiO_3$(ST)/$BaTiO_3$(BT) superlattice structure grown on the $SrTiO_3$ substrate under the fully commensurate constrained condition, the "hard domains" exhibits square-shaped hysteresis loop, however, when the thin film was partially relaxed, the domain wall width is much larger and the soft domains greatly reduced the coercive field of the superlattice.

In this paper, we first simulated a 2-domain structure of ferroelectric superlattice ST_4/BT_8, the polarization profiles across the domain wall of ST/interface/BT layers of superlattice ST_4BT_n (n = 1–8) are carefully examined by phase field model. Furthermore, we calculated the domain wall width as a function of temperature for the three layers. A temperature versus stacking structures phase diagram was depicted to distinguish the hard and soft domains state. This work also illustrated typical hard/soft domain wall profiles and these domain structures exhibit quite different hysteresis loops.

2. Phase Field Method

In the phase-field modeling of BT/ST superlattice heterostructures, the local polarization P is chosen as the order parameter to describe the ferroelectric domain structure of

*This paper was originally submitted to the Special Issue on Ferroic Domains and Related Functionalities organized by Xueyun Wang, Houbing Huang, Jing Wang and Zhonghui Shen.

†Corresponding author.

the superlattice. For studying polarization distribution around the ferroelectric domain wall, one simple three-dimensional (3D) model containing two domain (c+/c−) structures is assumed to be the initial domain structure. Note that the periodical boundary condition is applied along all the x, y and z directions, meaning that a multi-domain ferroelectric superlattice is performed in this simulation.

To describe the temporal evolution of the spatial distribution of the polarization vectors, time-dependent Ginzburg–Landau (TDGL) equations are employed,

$$\frac{\partial P_i(x,t)}{\partial t} = -L\frac{\delta F}{\delta P_i(x,t)} \quad (i=1,2,3), \tag{1}$$

where P_i is the ferroelectric polarization component, $x = (x_1, x_2, x_3)$ is the coordinate, t is time, L is the kinetic coefficient related to the domain evolution, F is the total free energy of the multi-domain ferroelectric superlattice and is given by

$$\begin{aligned} F = {} & F_{\text{bulk}}(P_i) + F_{\text{grad}}(\partial P_i / \partial x_j) \\ & + F_{\text{elast}}(P_i, \varepsilon_{ij}) + F_{\text{elec}}(P_i, E_i), \end{aligned} \tag{2}$$

where F_{bulk} is the bulk chemical energy, which can be shown as follows:

$$\begin{aligned} F_{\text{bulk}}(P_i) = \int_v \Bigg[& \frac{1}{2}\alpha_{ij}P_iP_j + \frac{1}{4}\gamma_{ijkl}P_iP_jP_kP_l \\ & + \frac{1}{6}\omega_{ijklmn}P_iP_jP_kP_mP_n \Bigg] d^3x, \end{aligned} \tag{3}$$

where α_{ij}, γ_{ijkl} and ω_{ijklmn} are the phenomenological Landau expression coefficients at zero external stress and zero external electric fields.

F_{grad} represents gradient energy:

$$F_{\text{grad}}\left(\frac{\partial P_i}{\partial x_j}\right) = \int_v \left[\frac{1}{2}G_{ijkl}\frac{\partial P_i}{\partial x_j}\cdot\frac{\partial P_k}{\partial x_l}\right] d^3x, \tag{4}$$

where G_{ijkl} is the gradient energy coefficient.

F_{elast} denotes elastic energy based on Khachaturyan's elastic theory:

$$F_{\text{elast}}(P_i, \varepsilon_{ij}) = \int_v \begin{bmatrix} \frac{1}{2}c_{ijkl}(\varepsilon_{ij} - Q_{ijkl}P_kP_l) \\ (\varepsilon_{kl} - Q_{klij}P_iP_j) \end{bmatrix} d^3x, \tag{5}$$

where ε_{ij} is the strain component. c_{ijkl} is the elastic stiffness tensor and Q_{ijkl} represents the electrostrictive coefficients.

F_{elec} is electrostatic energy:

$$F_{\text{elec}}(P_i, E_i) = -\int_v \left(\frac{1}{2}k_b\varepsilon_0 E_i^2 + E_iP_i\right) d^3x, \tag{6}$$

where E_i is the total electric field and ε_0 is the vacuum permittivity.

To simulate the superlattice structure, with the concept of phase field, one can use an order parameter η to distinguish the BT phase and ST phase, $\eta(r) = 1$ represents position r is occupied by ferroelectric BT phase while $\eta(r) = 0$ represents position r is occupied by paraelectric ST phase. For the interface region, η is set to 0.5. The Landau coefficients, elastic coefficients and electrostrictive coefficients for the superlattice system can be calculated using the 'rule of mixtures', for example, $\alpha_1(r) = \eta(r) \times \alpha_1\,(\text{BT}) + (1 - \eta(r)) \times \alpha_1(\text{ST})$, therefore, for the BT phase, $\alpha_1 = \alpha_1(\text{BT})$ and the ST phase $\alpha_1 = \alpha_1(\text{ST})$, at the interface region, $\alpha_1 = 0.5 \times (\alpha_1(\text{BT}) + \alpha_1(\text{ST}))$.

In this work, the polarization profile, i.e., the curve of polarization versus coordinate, is fitted with the hyperbolic tangent function:

$$P = P_s \tanh\left(\frac{x - x_0}{w}\right), \tag{7}$$

where P_s is the saturation polarization at the center of the ferroelectric domain. x_0 represents the position of the center of the ferroelectric domain wall. Thus, w is half of the domain wall thickness. In the simulation, we use the Octave program with a nonlinear curve fitting package to fit the domain wall in the BT phase.

Here, we discretized the simulation cell using $16\Delta x \times 16\Delta y \times N\Delta z$, with grid size $\Delta x = \Delta y = 1$ nm, $\Delta z = 0.2$ nm,

Table 1. The elastic coefficients, the electrostrictive coefficient, the lattice parameter and the Landau expression coefficients of the bulk free energy of $SrTiO_3$ and $BaTiO_3$. All the coefficients and parameters are in SI units.

Parameter	BT	ST
C_{11}	1.78×10^{11}	3.36×10^{11}
C_{12}	0.964×10^{11}	1.07×10^{11}
C_{44}	1.22×10^{11}	1.27×10^{11}
Q_1	0.10	0.066
Q_{12}	−0.034	−0.0135
Q_{44}	0.029	0.0096
a	$3.9994 \times 10^{-10} + 5.35386 \times 10^{-15}(T - 273)$	3.9043×10^{-10} [1+9.39]$\times 10^{-6}(T-273)+1.97 \times 10^{-9}(T-273)^2$]
α_1	$4.124(T - 388) \times 10^5$	$2.6353[\coth(42/T) - 0.90476] \times 10^7$
α_{11}	-2.097×10^8	1.696×10^9
α_{12}	7.974×10^8	1.373×10^9
α_{111}	1.294×10^9	
α_{112}	-1.950×10^9	
α_{123}	-2.500×10^9	
α_{1111}	3.863×10^{10}	
α_{1112}	2.529×10^{10}	
α_{1122}	1.637×10^{10}	
α_{1123}	1.367×10^{10}	

and $N = 2(n + m)$ for BT_n/ST_m superlattice structure. The grid size is related to real size via calculating domain wall energy. The Devonshire's bulk free energy coefficients, lattice parameters and electrostrictive and elastic coefficients for $SrTiO_3$ and $BaTiO_3$ employed in this work are listed in Table 1.[31–33]

3. Results and Discussion

Figures 1(a) and 1(b) show cross-sectional polarization vector distribution and the ferroelectric domain structure of a stable sample superlattice structure ST_4BT_8 at room temperature. The 2-domain structure with polarization towards $+z$ and $-z$ directions were initially constructed and then relaxed to a stable state. The tetragonal c+/c− domains were observed in both ST and BT layers, demonstrating the tetragonal phase structure was favored by the superlattice at room temperature. It should be noted that the ferroelectric material $SrTiO_3$ is in the cubic paraelectric phase at room temperature. This means that the polarizations observed in the ST layer is induced by the effect of electrostatic energy.

To clarify the domain wall structure, we plotted three polarization profiles across the film cross-sections, including the respective internal plane of the ST layer and BT layer and the ST/BT interface, as shown in Figs. 2(a)–2(c), respectively. Ising-like domain walls are observed in the middle of the ST layer and BT layer, as shown in Figs. 2(a) and 2(c), the polarization component in the transverse direction (P_x) and normal direction (P_y) are zero across the domain wall. Here, note that in the middle of the BT layer, a very sharp change of polarization results in narrow domain wall width.

The polarization in the ST layer is strongly affected by the stacking structure of the ST/BT superlattice. As mentioned above, the induced polarization in the ST layer is very sensitive to the thickness of the ST and BT layer, as the electrostatic boundary conditions can be complicated for different superlattice stacking structures. In the phase field model, as shown in Fig. 2(a), the value of polarizations in the ST layer is smaller than those in the BT layer, and we noticed that the induced polarization gradually switched from $+P_z$ to $-P_z$.

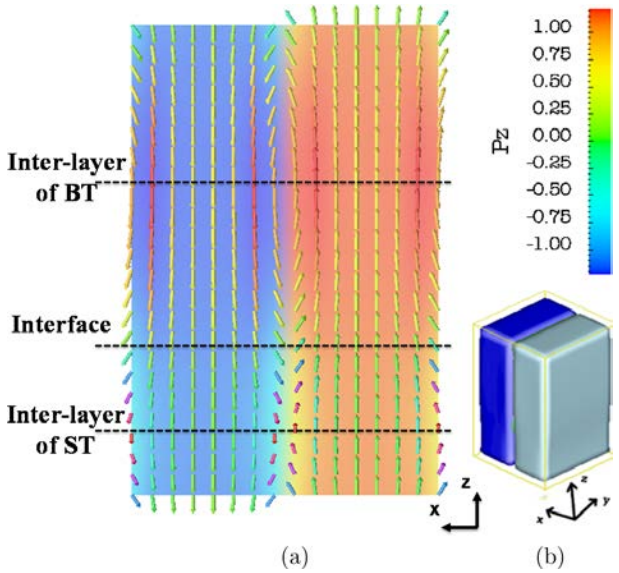

Fig. 1. (a) The cross-sectional polarization vector distribution and (b) the ferroelectric domain structure of a stable sample superlattice structure ST_4BT_8 simulated at room temperature.

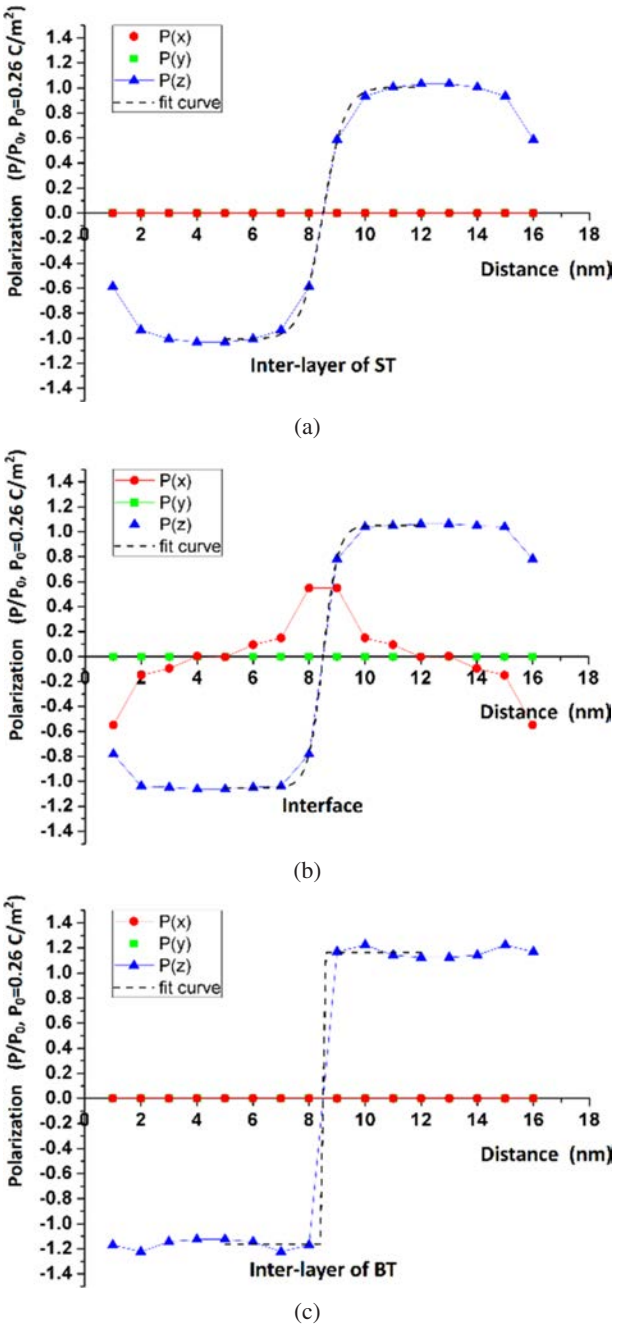

Fig. 2. The polarization components across the domain walls: (a) The inter-layer of ST, (b) the ST/BT interface and (c) the inter-layer of BT. The position of the measured curves is indicated by dashed lines in Fig. 1. Dashed lines represent fitted curves with hyperbolic tangent functions.

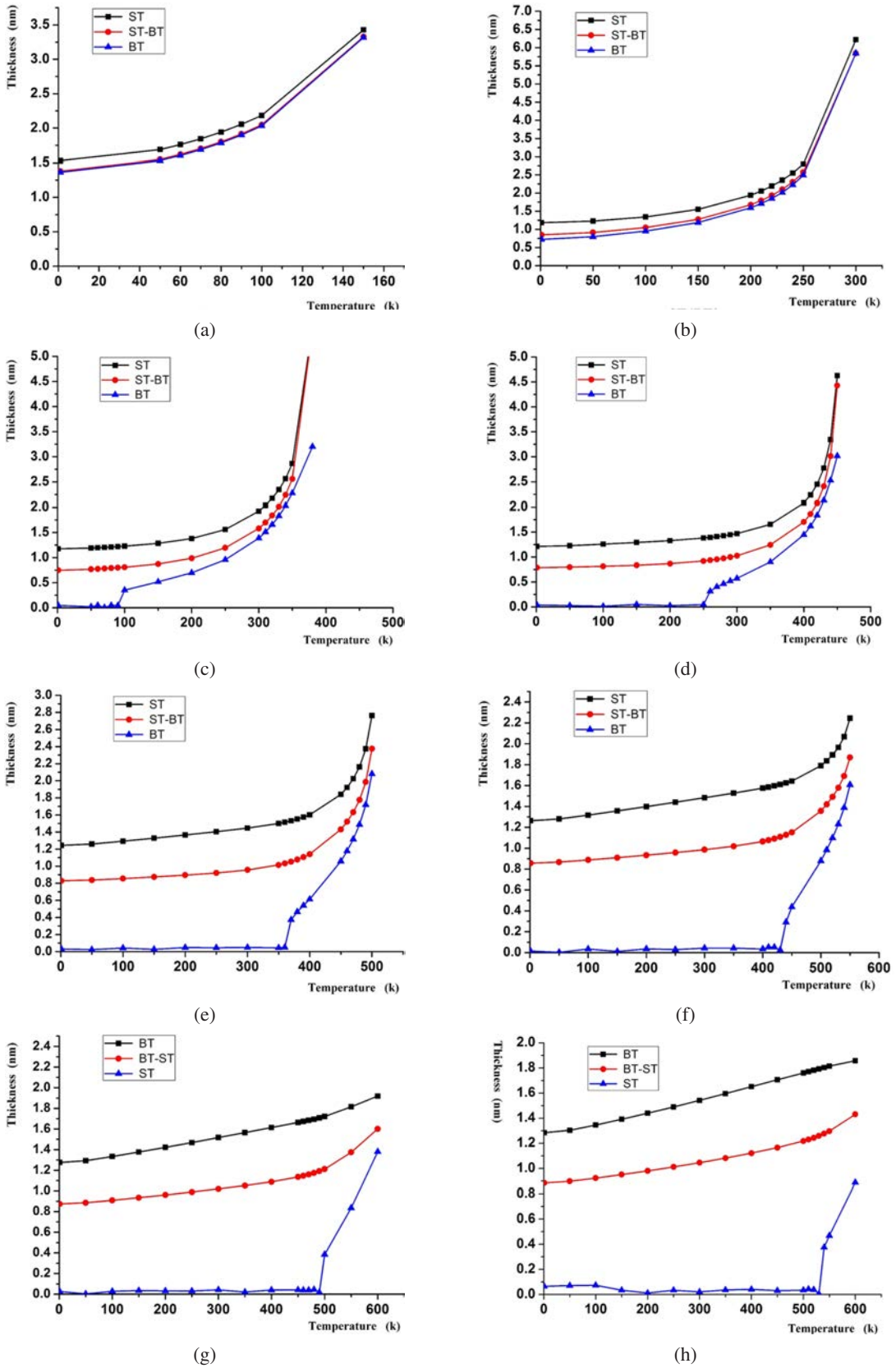

Fig. 3. The temperature dependence of domain wall width in ST/interface/BT layer of super lattice ST_4BT_n. (a)–(h) represents the measured superlattice structure $n = 1 - 8$, respectively.

This led to an increase in the domain wall width of the ST layer.

A mixed Ising–Néel wall was observed at the ST/BT interface.[18] As shown in Fig. 2(b), the polarization component along the normal direction (P_y) can be seen at the domain wall, indicating that the polarization rotates out of the cross-section plane and create a Néel-like domain wall, whereas the absolute value of the total polarization decreases when it passes through the domain wall, which suggests that the domain wall is an Ising–Néel mixed structure. Another interesting result obtained by our simulation is a pair of vortex/anti-vortex polarization configurations was formed in the center of the BT and ST layers. Considering that recent progresses in the topological structures in ferroelectric films/nanoislands[9–15] have been pursued, these topological textures can be achieved or controlled by carefully adjusting the stacking structure or the substrate of the superlattice.

The width of the domain wall is directly related to the ferroelectric domain structure and the switching dynamics. The domain wall profile in the BT phase was studied in the "Kittel-approximation",[25–28] the thickness of the domain wall can be ultra-thin (smaller than 1 nm) in the simulation. In this case, the domain wall is difficult to move and the "hard domain" state was generated. While in the ST layer, or when the ferroelectric is close to the transition temperature, a gradual polarization profile distribution can be observed, which leads to the appearance of a "soft domain" state, where the sinusoidal-like polarization makes it possible to move domain walls easily.

To measure the width of the domain wall, the hyperbolic tangent function (Eq. (7)) is used to fit out the domain wall thickness. The fitted curves are indicated by dashed lines in Fig. 2. In this work, for simplicity, we kept the thickness of the ST layer constant and change the thickness of the BT layer to investigate the polarization profiles of ST_4BT_n, where n is from 1 to 8. The temperature variation of domain wall width for superlattice structure ST_4BT_n (n = 1–8) is shown in Figs. 3(a)–3(h), respectively. Figures 4(a)–4(d) present some selected polar textures of BT_n/ST_4 (n = 2, 4, 6, 8) superlattice at room temperature. If n = 1 or 2, only the soft domain state can be observed in both the ST and BT layers. For n> =3, at low temperatures, the domain wall width in the BT layer is very close to zero, this feature can be used for the identification of a Kittel-like domain state. More interestingly, the vortex/anit-vortex structure was found in the simulation, as indicated in the red/blue boxes in Fig. 4. The direction of polarization favors energetically in parallel to the interface plane at the BT/ST interfaces, resulting in the formation of a vortex/anti-vortex texture in the superlattice. As the BT layer thickness increases, the vortex structure is elongated along the z-axis, but there is no significant change in the anti-vortex structure.

When temperature increases, the transition from hard to soft domain wall state occurs at a transition temperature T_r, which can be indicated by a discontinuous jump in domain

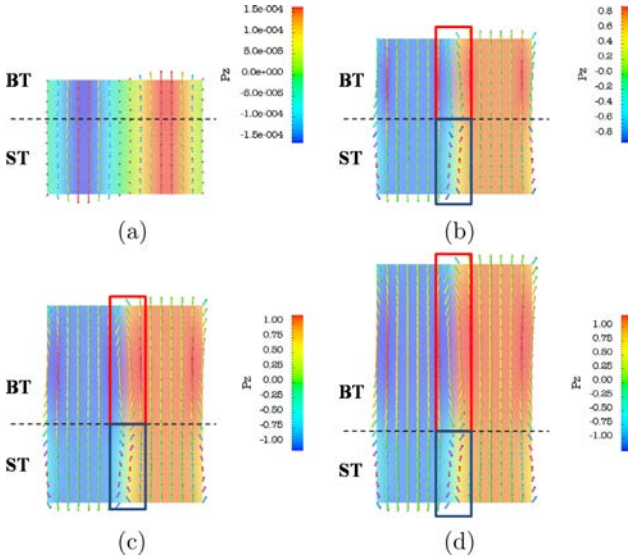

Fig. 4. The cross-sectional polarization vector distribution of superlattice ST_4BT_n, (a)–(d) represents the polar texture for ST_4BT_2, ST_4BT_4, ST_4BT_6 and ST_4BT_8, respectively.

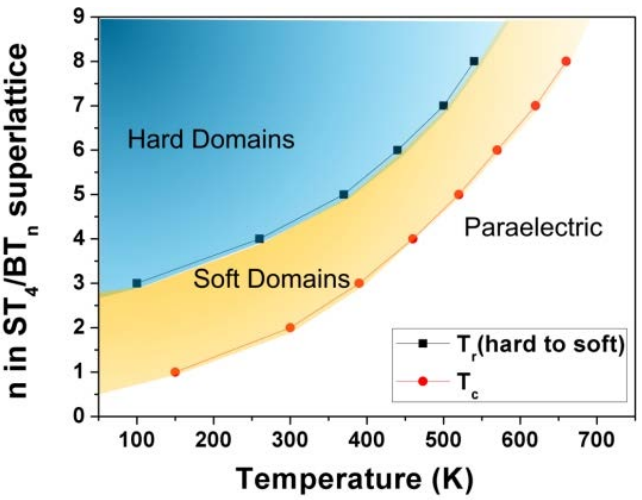

Fig. 5. (Color online) A domain wall state phase diagram as a function of temperature and the thickness of BT layer for superlattice ST_4BT_n. Black squared and red dotted lines denote the transition temperature T_r and the Curie temperature T_c of the ferroelectric superlattice, respectively.

wall width. The temperature played an important role in the transition of the hard domain state to the soft domain state. When increasing the temperature, the spontaneous polarization in the BT phase decreases. It should be noted that the reduction of the polarization appears to be larger near the domain wall to lower the electrostatic energy of the superlattice, which directly induced the broadening of domain walls, resulting in a domain wall state switching from the hard domain to the soft domain. Further increases the temperature, the superlattice quickly transfers to the paraelectric phase at the critical temperature T_c.

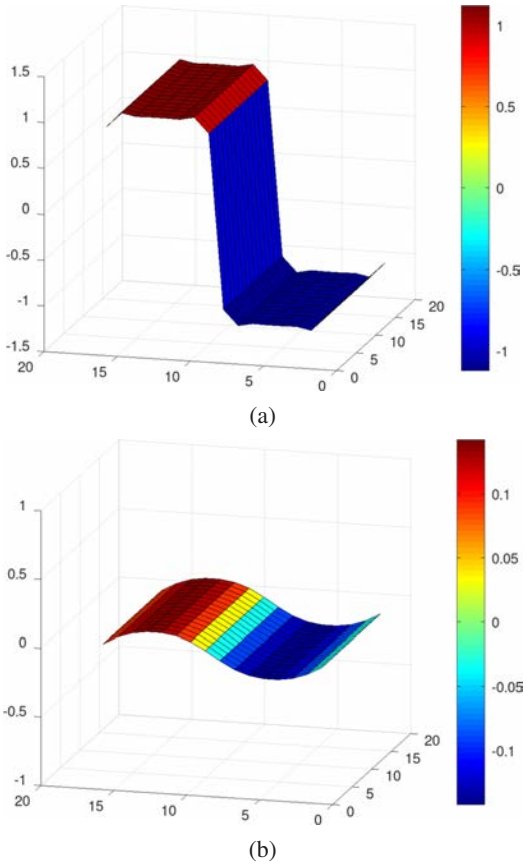

Fig. 6. Polarization profile (a) for hard domain wall (in BT layer of ST_4BT_8) and (b) for soft domain wall (in BT layer of ST_4BT_2) at 300 K.

With the two transition temperatures T_r and T_c, one can construct a domain wall state phase diagram as a function of BT layer thickness and temperature, as shown in Fig. 5. The black squared line separates the hard domain state and soft domain state in the BT layers, and the red dotted line separates the soft domain state and paraelectric state. Here, note that the polarization profile in the ST layer always contains soft domains as it was induced by the electrostatic effect. With increasing temperature or reducing the thickness of BT layers, the tetragonal c+/c− domains of the BT layer will shift from a Kittle-like hard domain state to a sinusoidal-like soft domain state at T_r and finally arrive at the paraelectric state at T_c.

A typical soft domain wall and hard domain wall profiles are illustrated in Fig. 6. When approaching T_c, with the decrease in the value of polarization, the domain wall state enters the soft domain state at T_r and the magnitude of polarization further decreases until the whole superlattice structure enters the paraelectric state.

Figure 7 shows the polarization hysteresis loops of superlattice ST_4BT_8 and ST_4BT_2 at room temperature. Hard domain walls in the superlattice structure improve the rectangularity of the hysteresis. It takes larger external fields to move the hard domain walls, resulting in higher remanent polarization and coercive field. In contrast, it is easier for soft domain walls to move, and the superlattice can reach saturation at a lower field.

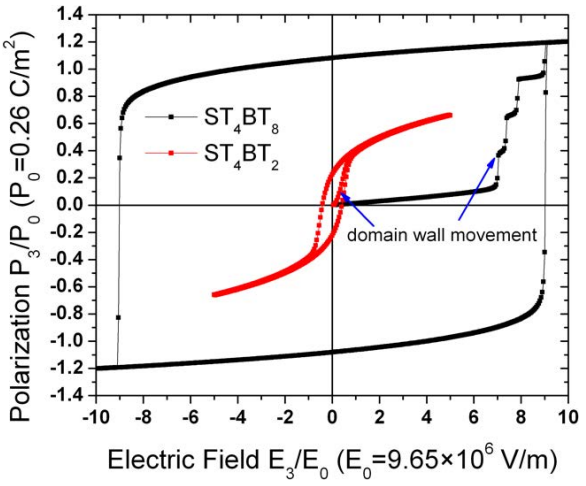

Fig. 7. (Color online) Simulated hysteresis loops for superlattice ST_4BT_8 (with hard domain walls) and ST_4BT_2 (with soft domain walls). Blue arrows point out the domain wall movement stage in the initial polarization process. Hard domain walls in the superlattice structure are more difficult to move, resulting in higher remanent polarization and coercive field.

4. Conclusions

Concerning the phase field simulation on the polarization profiles and domain wall structure of superlattice $SrTiO_3$/$BaTiO_3$, the following remarked features should be addressed:

(i) The polarization profile at the domain wall can be Kittel-like (hard) or sinusoidal-like (soft). In the BT/ST superlattice structure, the domain wall state in the BT layer can be hard or soft depending on the temperature or superlattice stacking structure. However, only the soft domain wall can be observed in the ST layer because the polarization in the ST layer was induced by the electrostatic field. The "hard domains" require larger applied fields to move and exhibit a square-shaped hysteresis loop.

(ii) The transition from hard domains to soft domains leads to a jump of domain wall width at transition temperature T_r. A domain wall state phase diagram can be constructed based on the transition temperatures T_r/T_c and the stacking structure of the superlattice. Using the diagram, one can expect and analyze the domain wall state in ST/BT superlattice structure on a given substrate.

(iii) Polar vortex/anti-vortex structure was observed in the BT layer and ST layer, respectively. Concerning recent development in topological textures of the superlattice structure, superlattice structures with topological textures have great potential for nonvolatile high-density memory devices.

These simulation results should motivate further exploration of ferroelectric superlattice structures. We hope that the phase field method will give the power tool for the prediction and analysis of new domain/domain wall structures of ferroelectric superlattice structures in the future.

Acknowledgment

This work was supported by the Advanced Functional Materials Research and Innovation Group of the Xiamen Institute of Technology (Grant Number KYTD202004).

References

[1]L. E. C. Alexander K. Tagantsev and J. Fousek, *Domains in Ferroic Crystals and Thin Films* (Springer, 2009).
[2]D. Damjanovic, Ferroelectric, dielectric and piezoelectric properties of ferroelectric thin films and ceramics, *Rep. Prog. Phys.* **61**, 1267 (1998).
[3]D. A. Tenne, A. Bruchhausen, N. D. Lanzillotti-Kimura, A. Fainstein, R. S. Katiyar, A. Cantarero, A. Soukiassian, V. Vaithyanathan, J. H. Haeni, W. Tian, D. G. Schlom, K. J. Choi, D. M. Kim, C. B. Eom, H. P. Sun, X. Q. Pan, Y. L. Li, L. Q. Chen, Q. X. Jia, S. M. Nakhmanson, K. M. Rabe and X. X. Xi, Probing nanoscale ferroelectricity by ultraviolet Raman spectroscopy, *Science* **313**, 1614 (2006).
[4]D. G. Schlom, L.-Q. Chen, C.-B. Eom, K. M. Rabe, S. K. Streiffer and J.-M. Triscone, Strain tuning of ferroelectric thin films, *Annu. Rev. Mater. Res.* **37**, 589 (2007).
[5]D. G. Schlom, L.-Q. Chen, X. Pan, A. Schmehl and M. A. Zurbuchen, A thin film approach to engineering functionality into oxides, *J. Amer. Ceram. Soc.* **91**, 2429 (2008).
[6]E. Bousquet, M. Dawber, N. Stucki, C. Lichtensteiger, P. Hermet, S. Gariglio, J. M. Triscone and P. Ghosez, Improper ferroelectricity in perovskite oxide artificial superlattices, *Nature* **452**, 732 (2008).
[7]A. Soukiassian, W. Tian, V. Vaithyanathan, J. H. Haeni, L. Q. Chen, X. X. Xi, D. G. Schlom, D. A. Tenne, H. P. Sun, X. Q. Pan, K. J. Choi, C. B. Eom, Y. L. Li, Q. X. Jia, C. Constantin, R. M. Feenstra, M. Bernhagen, P. Reiche and R. Uecker, Growth of nanoscale $BaTiO_3/SrTiO_3$ superlattices by molecular-beam epitaxy, *J. Mater. Res.* **23**, 1417 (2011).
[8]A. S. Sidorkin, L. P. Nesterenko, Y. Gagou, P. Saint-Gregoire, E. V. Vorotnikov, A. Y. Pakhomov and N. G. Popravko, Repolarization of ferroelectric superlattices $BaZrO_3/BaTiO_3$, *Sci. Rep.* **9**, 18948 (2019).
[9]P. Wu and Y. Liang, Lattice phase field model for nanomaterials, *Materials (Basel)* **14**, 7317 (2021).
[10]Z. Hong, S. Das, C. Nelson, A. Yadav, Y. Wu, J. Junquera, L. Q. Chen, L. W. Martin and R. Ramesh, Vortex domain walls in ferroelectrics, *Nano. Lett.* **21**, 3533 (2021).
[11]C. Tan, Y. Dong, Y. Sun, C. Liu, P. Chen, X. Zhong, R. Zhu, M. Liu, J. Zhang, J. Wang, K. Liu, X. Bai, D. Yu, X. Ouyang, J. Wang, P. Gao, Z. Luo and J. Li, Engineering polar vortex from topologically trivial domain architecture, *Nat. Commun.* **12**, 4620 (2021).
[12]J. Kim, M. You, K.-E. Kim, K. Chu and C.-H. Yang, Artificial creation and separation of a single vortex–antivortex pair in a ferroelectric flatland, *npj Quantum Mater*. **4**, 29 (2019).
[13]S. Estandia, F. Sanchez, M. F. Chisholm and J. Gazquez, Rotational polarization nanotopologies in $BaTiO_3/SrTiO_3$ superlattices, *Nanoscale* **11**, 21275 (2019).
[14]A.Y. Abid, Y. Sun, X. Hou, C. Tan, X. Zhong, R. Zhu, H. Chen, K. Qu, Y. Li, M. Wu, J. Zhang, J. Wang, K. Liu, X. Bai, D. Yu, X. Ouyang, J. Wang, J. Li and P. Gao, Creating polar antivortex in $PbTiO_3/SrTiO_3$ superlattice, *Nat. Commun.* **12**, 2054 (2021).
[15]Y. J. Wang, Y. P. Feng, Y. L. Zhu, Y. L. Tang, L. X. Yang, M. J. Zou, W. R. Geng, M. J. Han, X. W. Guo, B. Wu and X. L. Ma, Polar meron lattice in strained oxide ferroelectrics, *Nat. Mater.* **19**, 881 (2020).
[16]Q. L. Yixuan Zhang, H. Huang, J. Hong and X. Wang, Strain manipulation of ferroelectric skyrmion bubbles in a freestanding $PbTiO_3$ film: A phase field simulation, *Phys. Rev. B* **105**, 224101 (2022).
[17]Q. Zhang, L. Xie, G. Liu, S. Prokhorenko, Y. Nahas, X. Pan, L. Bellaiche, A. Gruverman and N. Valanoor, Nanoscale bubble domains and topological transitions in ultrathin ferroelectric films, *Adv. Mater.* **29**, 1702375 (2017).
[18]D. Lee, R. K. Behera, P. Wu, H. Xu, Y. L. Li, S. B. Sinnott, S. R. Phillpot, L. Q. Chen and V. Gopalan, Mixed Bloch-Néel-Ising character of 180° ferroelectric domain walls, *Phys. Rev. B.* **80**, 060102 (2009).
[19]E. A. Eliseev, A. N. Morozovska, S. V. Kalinin, Y. Li, J. Shen, M. D. Glinchuk, L.-Q. Chen and V. Gopalan, Surface effect on domain wall width in ferroelectrics, *J. Appl. Phys.* **106**, 084102 (2009).
[20]G. Catalan, J. Seidel, R. Ramesh and J. F. Scott, Domain wall nanoelectronics, *Rev. Mod. Phys.* **84**, 119 (2012).
[21]M. Li, Y. Gu, Y. Wang, L.-Q. Chen and W. Duan, First-principles study of 180° domain walls in $BaTiO_3$: Mixed Bloch-Néel-Ising character, *Phys. Rev. B* **90**, 054106 (2014).
[22]M. Wang, T. Xia and L. D. Geng, Phase-field study of crystallographic texturing in piezoelectric polycrystals, *J. Adv. Dielec.* **12**, 2244002 (2022).
[23]Y. H. Shin, I. Grinberg, I. W. Chen and A. M. Rappe, Nucleation and growth mechanism of ferroelectric domain-wall motion, *Nature* **449**, 881 (2007).
[24]S. Choudhury, Y. Li, N. Odagawa, A. Vasudevarao, L. Tian, P. Capek, V. Dierolf, A. N. Morozovska, E. A. Eliseev, S. Kalinin, Y. Cho, L.-Q. Chen and V. Gopalan, The influence of 180° ferroelectric domain wall width on the threshold field for wall motion, *J. Appl. Phys.* **104**, 084107 (2008).
[25]F. De Guerville, I. Luk'yanchuk, L. Lahoche and M. El Marssi, Modeling of ferroelectric domains in thin films and superlattices, *Mater. Sci. Eng. B* **120**, 16 (2005).
[26]V. A. Stephanovich, I. A. Luk'yanchuk and M. G. Karkut, Domain-enhanced interlayer coupling in ferroelectric/paraelectric superlattices, *Phys. Rev. Lett.* **94**, 047601 (2005).
[27]F. De Guerville, M. El Marssi, I. Lukyanchuk and L. Lahoche, Ferroelectric domains in thin films and superlattices: Results of numerical modeling, *Ferroelectrics* **359**, 14 (2007).
[28]I. A. Luk'yanchuk, L. Lahoche and A. Sene, Universal properties of ferroelectric domains, *Phys. Rev. Lett.* **102**, 147601 (2009).
[29]P. Wu, X. Ma, Y. Li, V. Gopalan and L.-Q. Chen, Dipole spring ferroelectrics in superlattice $SrTiO_3/BaTiO_3$ thin films exhibiting constricted hysteresis loops, *Appl. Phys. Lett.* **100**, 092905 (2012).
[30]P. Wu, X. Ma, Y. Li, C.-B. Eom, D.G. Schlom, V. Gopalan and L.-Q. Chen, Influence of interfacial coherency on ferroelectric switching of superlattice $BaTiO_3/SrTiO_3$, *Appl. Phys. Lett.* **107**, 122906 (2015).
[31]J. Schubert, O. Trithaveesak, A. Petraru, C. L. Jia, R. Uecker, P. Reiche and D. G. Schlom, Structural and optical properties of epitaxial $BaTiO_3$ thin films grown on $GdScO_3$(110), *Appl. Phys. Lett.* **82**, 3460 (2003).
[32]Y. L. Li, S. Y. Hu, D. Tenne, A. Soukiassian, D. G. Schlom, L. Q. Chen, X. X. Xi, K. J. Choi, C. B. Eom, A. Saxena, T. Lookman and Q. X. Jia, Interfacial coherency and ferroelectricity of $BaTiO_3/SrTiO_3$ superlattice films, *Appl. Phys. Lett.* **91**, 252904 (2007).
[33]Y. L. Li, S. Y. Hu, D. Tenne, A. Soukiassian, D. G. Schlom, X. X. Xi, K. J. Choi, C. B. Eom, A. Saxena, T. Lookman, Q. X. Jia and L. Q. Chen, Prediction of ferroelectricity in $BaTiO_3/SrTiO_3$ superlattices with domains, *Appl. Phys. Lett.* **91**, 112914 (2007).